Local magnetic effects of interface alloying in Fe/Co superlattices

2006 J. Phys.: Condens. Matter 18 5807

(http://iopscience.iop.org/0953-8984/18/26/002)

INSTITUTE OF PHYSICS PUBLISHING JOURNAL OF PHYSICS: CONDENSED MATTER

J. Phys.: Condens. Matter **18** (2006) 5807–5824 doi:10.1088/0953-8984/18/26/002

Local magnetic effects of interface alloying in Fe/Co superlattices

S Kamali-M[1], A Bergman[1], G Andersson[1], V Stanciu[2] and L Häggström[1]

[1] Department of Physics, Uppsala University, Box 530, SE-751 21 Uppsala, Sweden
[2] Department of Engineering Sciences, Uppsala University, Box 534, SE-751 21 Uppsala, Sweden

E-mail: Lennart.Haggstrom@fysik.uu.se

Received 20 December 2005, in final form 20 April 2006
Published 16 June 2006
Online at stacks.iop.org/JPhysCM/18/5807

Abstract

Effects of interface alloying and the thickness dependence of magnetic properties of Fe/Co(001) multilayers have been investigated. The thicknesses of the Fe layers have been varied between two and 14 monolayers while the Co layers have been held constant at 7 ML. From conversion electron Mössbauer spectroscopy (CEMS) measurements and electronic structure calculations it is found that the magnitude of the Fe magnetic hyperfine field is larger close to the interface and smaller in the middle of thick ($\geqslant$9 ML) Fe layers. For a thinner Fe layer ($\leqslant$5 ML) the largest field is found in the centre of the Fe layer. By modelling the effects of interface alloying from earlier data for bulk Fe–Co alloys, and comparing with the experimental results, the degree of interface alloying is estimated to be 2–3 ML at each interface.

1. Introduction

Although far from new, the combination of iron and cobalt continues to attract considerable interest in materials research, especially in the field of applied magnetism. One of the reasons for this is the very large magnetic moment per atom, and macroscopic magnetization, obtained in Fe–Co alloys with approximately 30 at.% Co, at the maximum of the Slater–Pauling curve [1]. Recently, information storage applications utilizing Fe–Co alloys have been proposed in theoretical papers [2].

In the past, a large number of local-probe studies have been devoted to bulk Fe–Co alloys and their magnetic properties [3–10]. As a natural continuation of this, in more recent years, the development in epitaxial deposition techniques has led to theoretical and experimental investigations of Fe/Co multilayers [11–19], with properties that in many respects are different from those of bulk samples. There are, however, quite a few discrepancies between the results from different experimental techniques in the previous studies. As an example, there are theoretical and experimental studies [13, 18, 19] that indicate that the magnetic moment of iron is increased in the interface regions, while the moments of Fe atoms far from the interface

regions are unaffected. This means that an iron atom sitting in the middle of a not-too-thin layer should have bulk-like properties. On the other hand, there are strong indications from Mössbauer spectroscopy that the hyperfine field, B_{hf}, of iron atoms far from an interface is larger than for the iron atoms in the interface regions [14, 15]. This ambiguity should be eliminated, which partly motivates further studies on Fe/Co multilayers.

Another aspect that is studied in the present paper is the influence of the local interface environment on the hyperfine fields of Fe atoms. This can be addressed conveniently by means of local probe methods, in the present case conversion electron Mössbauer spectroscopy (CEMS). The interface structure is of utmost importance for several properties of multilayers and superlattices (here used as denoting single-crystal-like multilayers), but there are still no straightforward methods for obtaining detailed information on, e.g., the sharpness of interfaces in metallic multilayers. On this particular point the main issue lies in distinguishing between chemically sharp interfaces between layers that vary slightly in thickness over length scales corresponding to a few atomic distances, i.e. roughness, and interfaces that are not chemically sharp but exhibit some alloying between the constituents, i.e. intermixing. Recently, investigations on how to model and deduce the chemical smearing of interfaces through comparison between (a) calculated and measured magnetic moments in Fe/V [20] and $Fe_{0.82}Ni_{0.18}$/V [21] superlattices and (b) magnetic hyperfine fields in Fe/V multilayers [22] were presented as routes toward resolving this issue. Now, collecting the information from a local probe technique of the environments of each iron atom, as well as average Fe–Co magnetic moments measured with absolute magnetometry, and calculating both with the aid of previous bulk and multilayer results, we may finally deduce both the width of the interface region that affects the iron moments, and how the hyperfine field on the Fe atoms varies within the multilayer structure.

This paper is structured as follows: after the experimental details, in the next section, the results will be presented. The subsequent section describes calculations of hyperfine fields and magnetic moments in Fe/Co multilayers with varying degree of alloying at the interfaces. Finally, the results will be discussed in greater detail.

2. Experimental details

The samples were prepared by dc magnetron sputtering in a UHV chamber previously described elsewhere [23], with a base pressure of 6×10^{-10} Torr (8×10^{-8} Pa) and 6–8 mTorr argon (99.999 95%) as sputtering gas. Each substrate, $20 \times 20 \times 1$ mm^3 MgO with (001) orientation, was annealed on the sample holder at 700 °C for 40 min. Then a buffer layer consisting of 50 Å Fe (99.95% purity and the natural 2% abundance of ^{57}Fe) was deposited at 330 °C to promote the growth of the Fe/Co superlattice [16, 19]. The temperature was subsequently lowered further to 200 °C, and the ^{57}Fe/Co superlattice structure was deposited through alternating sputtering from ^{57}Fe and Co targets of 99.95% purity, with the first and last layers being Co. The ^{57}Fe target consisted of a very thin slice of isotope-enriched pure Fe (95% ^{57}Fe) put on top of an especially designed target backing plate of natural Fe. Finally, the superlattice was covered by approximately 10 Å Pd to prevent oxidation.

A series of samples was prepared in this manner, keeping the Co thickness constant at seven monolayers (ML), corresponding to approximately 10 Å, and varying the ^{57}Fe thickness, L_{Fe}, from 2 to 14 ML. The superlattices with lower L_{Fe} contained a slightly higher number of bilayer repetitions to increase the total amount of ^{57}Fe. The number of repetitions, N, and the Fe thickness for each sample is given in table 1. The notation used for the samples in this paper is x/y where x stands for the number of Fe monolayers and y for the number of Co monolayers, which is constant and equal to 7 ML.

Table 1. n_{Fe} and N are the nominal number of Fe monolayers and number of bilayer repetitions. The Co thickness was nominally constant, 7 ML. d_{exp} is the experimental average monolayer thickness through the whole superlattice and Λ_{exp} is the experimental bilayer thickness in monolayers, which is calculated by dividing Λ_{exp} in Å by d_{exp}. μ_{exp} is the average atomic magnetic moment in the Fe/Co bilayers.

n_{Fe} (ML)	N	Fe buffer (Å)	d_{exp} (Å)	Λ_{exp} (ML)	μ_{exp} (μ_B) at 10 K	μ_{exp} (μ_B) at 300 K
2	24	50	1.413	9.7	1.98	1.95
3	20	50	1.414	11.7	2.17	2.15
5	21	100	1.411	12.8	2.27	2.25
9	18	50	1.420	18.7	2.17	2.13
14	18	50	1.420	24.4	1.97	1.93

The structural quality of the films was investigated by x-ray diffraction using a Siemens/Bruker D5000 in Bragg–Brentano geometry with a Cu Kα source whose wavelength is 1.5406 Å.

For the alloy reference samples high purity (99.99%) Fe and Co were arc melted and homogenized in a high frequency induction furnace in Ar atmosphere. The following compositions were made: $Fe_{0.75}Co_{0.25}$, $Fe_{0.50}Co_{0.50}$ and $Fe_{0.25}Co_{0.75}$. The samples were subsequently held at 800 °C in vacuum in for 7 days and then quenched to room temperature. Mössbauer absorbers were made from powder filings of the ingots mixed with boron nitride.

For ^{57}Fe Mössbauer spectroscopic measurements, ^{57}Co in Rh at room temperature was used as source. The spectra were calibrated by using the six lines of α-Fe. The centre of the α-Fe spectrum was taken as zero isomer shift. All the conversion electron Mössbauer spectroscopy (CEMS) measurements were made at room temperature, using a gas flow (He and CH_4) detector. The direction of the incoming photons was perpendicular to the sample plane.

Conventional transmission Mössbauer spectra at room temperature were recorded for the alloy samples.

Absolute magnetization measurements at 10 K and at 300 K were performed using a Quantum Design MPMS XL SQUID (superconducting quantum interference device) magnetometer. For these measurements, pieces of approximate size 3×3 mm^2 were cut from the original samples. The external field was applied in the film plane, (001), and the magnetization was measured along the sample edge which corresponds to the Fe/Co [110] direction.

3. Experimental results

3.1. XRD results

As an example, the x-ray reflectivity (XRR) and the x-ray diffraction (XRD) measurements of sample 14/7 are shown in figure 1.

Beside the (002) superlattice peak, bilayer satellites are observed in all samples except in the 2/7 sample, where they, if present, fall into the background intensity. This indicates that strong intermixing has occurred in the 2/7 sample. The high-angle satellite positions were used to obtain experimental values of the chemical periodicity, Λ, except for the 2/7 sample, where the reflectivity superlattice peak was used instead. Here it should be clarified that only one reflectivity peak is observed for 2/7, further supporting a very weak periodic variation in electron density in that sample. The position of the Fe/Co (002) Bragg peak, indicated in

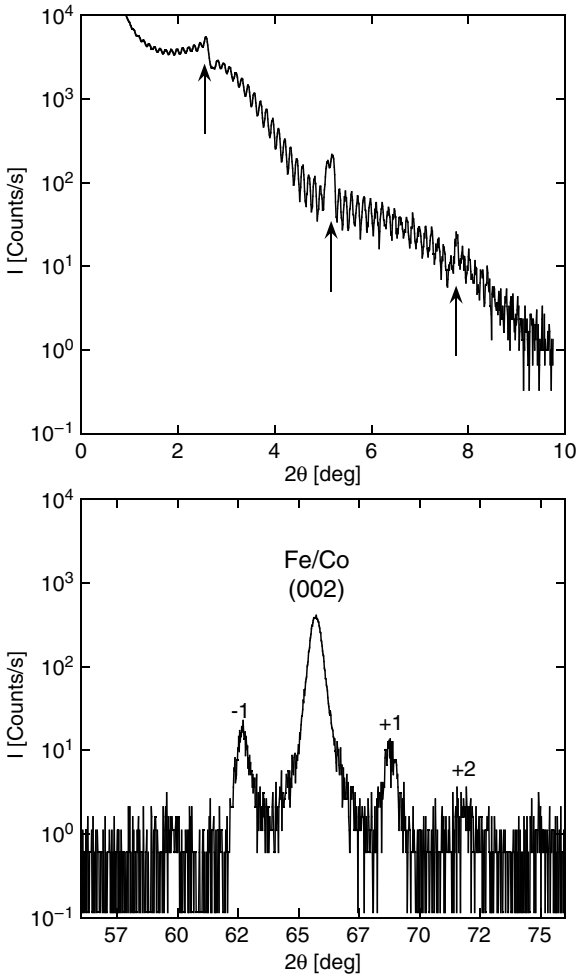

Figure 1. The XR reflectivity curve (upper) where the arrows indicate the chemical modulation peaks and XR diffraction (lower) where the Fe/Co (002) peak together with its satellites are shown for sample 14/7.

figure 1, yielded the out-of-plane atomic distance, d_{exp}, given in table 1. The experimentally found results for the average lattice constants are displayed in figure 2 and will be discussed later. The experimental number of monolayers in each bilayer, also given in table 1, was obtained through dividing the experimental Λ values by d_{exp}. The bilayer thicknesses and the total thicknesses differ from the nominal values as can be seen in table 1. The relatively low intensities of the diffraction satellites and the reflectivity Bragg peaks are due to the poor contrast between Fe and Co in x-ray scattering.

3.2. SQUID results

The SQUID measurements performed at 10 and 295 K for the 5/7 and 14/7 samples are given in figure 3. To account for the buffer layer, we used 2.176 and 2.218 μ_{B}/atom for the Fe magnetic moment at 295 and 10 K, respectively [27]. The results from the SQUID

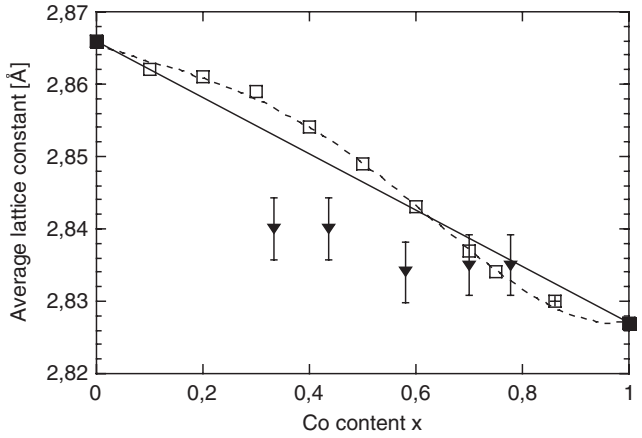

Figure 2. The average lattice constants of $Fe_{1-x}Co_x$ alloys versus Co concentration, together with the values from the present superlattices (calculated from the formula $(a^2c)^{1/3}$ where $a = 2.84$ Å and $c = 2d_{exp}$ are the in- and out-of-plane lattice constants, respectively). Values are from [24] (open squares), from [25] (filled square at $x = 1$), from [26] (filled square at $x = 0$), from [15] (cross) and from the present superlattices (filled triangles).

magnetometry, calculated from the saturation magnetization to give the moment per 'FeCo' atom, are summarized in table 1. The easy magnetization directions were along the in-plane [110] axes for all samples, except for the 14/7 sample, where the easy axes were along the in-plane [100] directions.

3.3. Mössbauer results

The experimental spectra for all *superlattice* samples and fit spectra using two or three subspectra, giving reasonable good fits, are shown in figure 4. All hyperfine parameters and subspectral intensities were fitted independently and are given in table 2. The intensity ratio between the line 2(5) and 1(3) is four for all samples, which means that the magnetic hyperfine fields are completely in the plane of the films. The fittings are done by a model with Gaussian distributions in the magnetic hyperfine fields, B_{hf}, and a fixed value of the individual Lorentzian linewidths of 0.26 mm s^{-1}. The magnetic hyperfine field distributions for all spectra are shown in figure 5. The magnitude of B_{hf} is used in this paper, realizing that B_{hf} is negative in the present samples.

The spectra of the *alloy samples* displayed a six line pattern with an asymmetry of line heights for the outer lines. Because of this, the spectra were fitted with two sextets, each with Gaussian distribution in the magnetic hyperfine field. The results are presented in figures 6 and 7 and in table 3.

4. Calculational details and results

Along with the experimental measurements, we have also calculated the hyperfine fields and the magnetization profile of selected multilayers (5/7 and 9/7) from first-principles electronic structure calculations. The calculations were performed using a real-space linear muffin tin orbital method within the atomic sphere approximation (RS-LMTO-ASA) [28]. This method is based on the Haydock recursion method [29] and is fully self-consistent within the local spin density approximation (LSDA) [30]. Relativistic effects are also taken into account

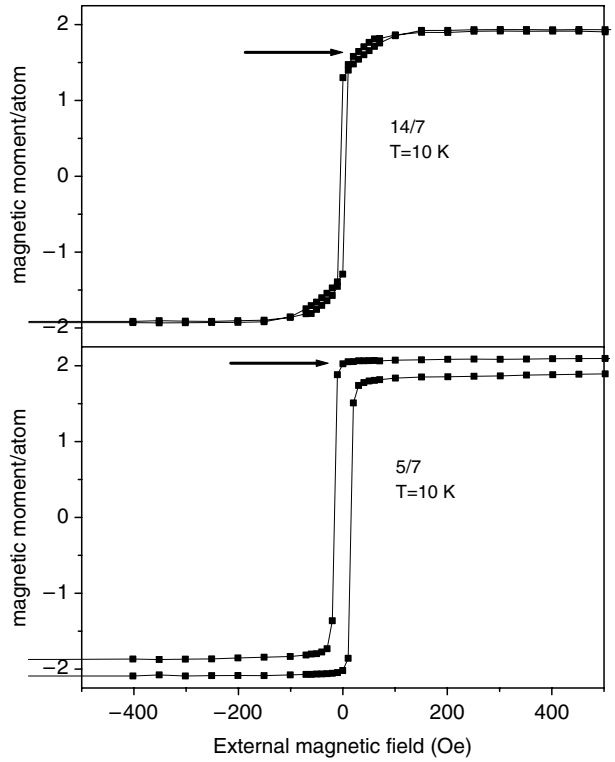

Figure 3. The magnetization curves from SQUID for the 14/7 (upper) and 5/7 (lower) samples. The shape of the curves when the external field is decreasing toward zero, marked by arrows, is different, which is an indication that the easy axis for the 5/7 sample is in the same direction as the applied field, i.e. the FeCo [110] direction, but for the 14/7 sample the easy axis is in the [100] direction.

with this method by including the spin–orbit coupling in the Hamiltonian. The continued fraction stemming from the recursion relation has been terminated with the Beer–Pettifor terminator [31] after 25 recursion steps and the multilayers have been simulated using clusters containing more than 10 000 atoms.

The hyperfine field was calculated by evaluating the Fermi contact contribution $B_{\mathrm{hf}} = \frac{2}{3}\mu_0\mu_{\mathrm{B}}[\rho^{\uparrow}(0) - \rho^{\downarrow}(0)]$ where $\rho^{\uparrow}(0)$ and $\rho^{\downarrow}(0)$ is the spin-up and spin-down densities at the nucleus. Contributions to the field from both core (1s, 2s and 3s) and valence (4s) electrons are calculated. The RS-LMTO-ASA method has previously been used for calculations of hyperfine fields and related quantities and details of how these calculations are performed can be found in more detail in references [32, 33]. We have also considered interface alloying in the multilayers by replacing Fe and Co layers close to the interface with random Fe–Co alloys having varying concentration profile. The concentration profile considered in this work was $Fe_{0.5}Co_{0.5}$ for the Fe interface layer, $Fe_{0.7}Co_{0.3}$ for the Fe layer next to the interface, and $Fe_{0.95}Co_{0.05}$ for Fe atoms two layers away from the interface. For the Co side the opposite concentration relation was used. The alloying has been modelled using the virtual crystal approximation (VCA), which is known to work well for Fe–Co systems [34].

In figure 9, the individual Fe magnetic moments for the 5/7 and 9/7 systems with both perfect and alloyed interfaces are shown. The calculated hyperfine fields for Fe atoms in the 5/7 and 9/7 systems are shown in figure 10.

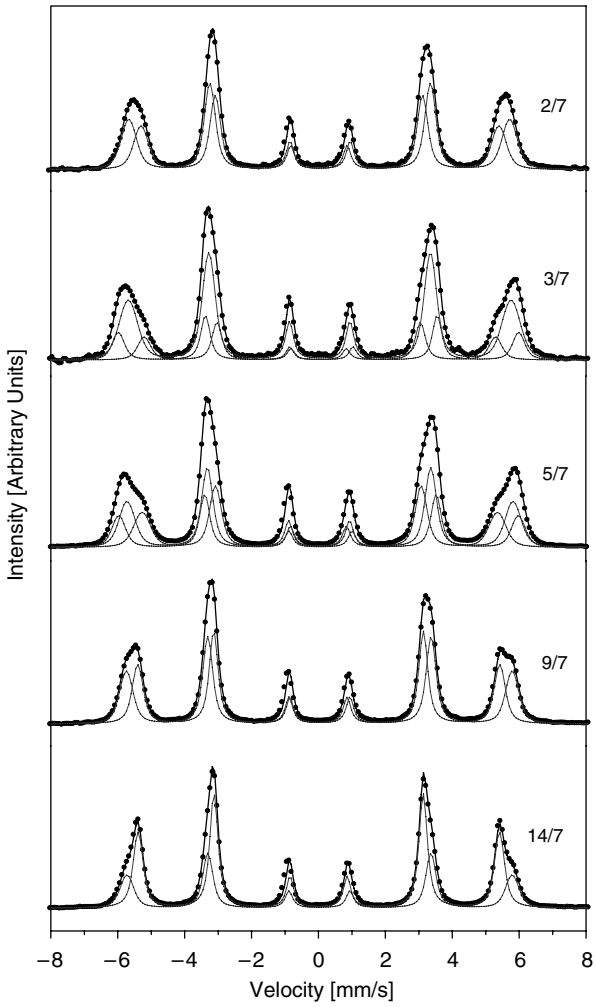

Figure 4. Mössbauer spectra of all samples denoted by x/y, where x and y stand for the nominal number of monolayers of Fe and Co, respectively.

5. Discussions

5.1. Lattice constants

The in-plane lattice constants have been shown to be controlled by the substrate. In previous studies the in-plane lattice parameters of multilayers grown on MgO has been determined to be $a = 2.84(1)$ Å [35]. According to table 1, $c = 2d_{\mathrm{exp}}$ is smaller than the Vegard's law straight line in figure 2. Since Vegard's law applies to atomic volume, the average lattice constant $(a^2c)^{1/3}$ was calculated for the present samples. As seen in figure 2, the 9/7 and 14/7 samples still deviate considerably from the straight line. It seems that an increase in the Co layer thickness by 2.7 and 3.4 ML as compared to the nominal values for the 9/7 and 14/7 samples, respectively, can bring the experimentally observed c values closer to what Vegard's law predicts. Hence it may be assumed that the discrepancy between the nominal and experimental number of monolayers, as seen in table 1, is mainly due to the deposition of

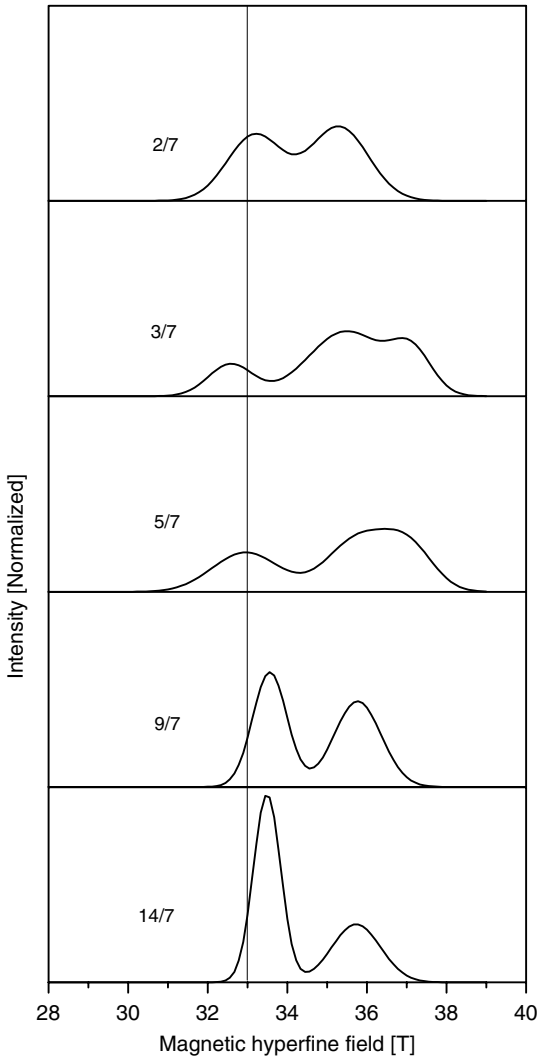

Figure 5. The Fe magnetic hyperfine field distributions for the different samples (table 2). The line indicates the magnetic hyperfine field for Fe atoms in α-Fe, which is 33.0 T.

thicker Co layers than intended. This in turn has to do with a generally observed increase over time in deposition rate from an individual sputtering target. Unfortunately, modelling of x-ray reflectivity for reliable determination of individual layer thicknesses is not feasible in this case due to the poor contrast and low numbers of monolayers in each period.

5.2. Experimental Fe magnetic hyperfine fields

Under this heading we discuss briefly the experimentally found Fe hyperfine field B_{hf} with respect to the variation of the effective magnetic hyperfine field at Fe nuclei versus Co concentration of $Fe_{1-x}Co_x$ alloys (figure 7). In section 6, a more detailed simulation approach will be made. The B_{hf} shows (figure 7) a marked maximum 36.6 T for $x \approx 0.27$, whereas on both sides of this x value the field decreases.

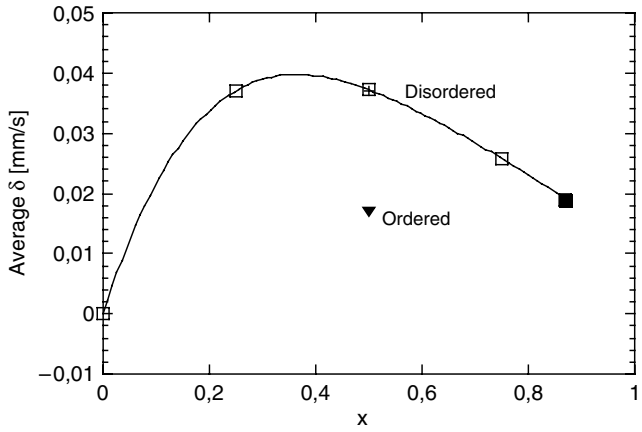

Figure 6. Average isomer shift for ^{57}Fe nuclei versus Co concentration of $Fe_{1-x}Co_x$ alloys. Values from [6] for the disordered phase as a cross and as a filled triangle for the ordered B2 phase, from [15] as a filled square and from the present alloy samples open squares.

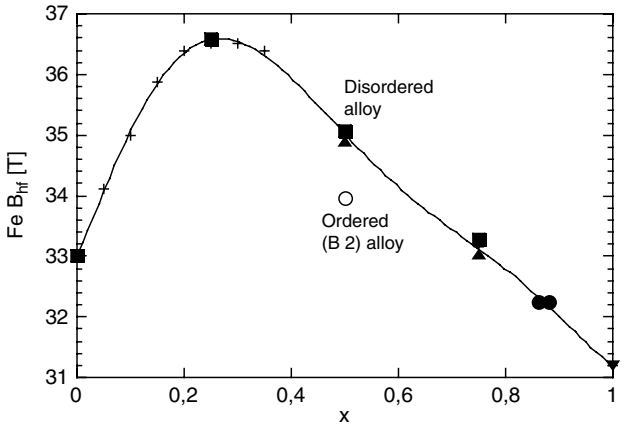

Figure 7. Experimental variation of the average magnetic hyperfine field at the ^{57}Fe nuclei versus Co concentration of $Fe_{1-x}Co_x$ alloys. Crosses from [4], upwards triangles and open circle from [8], downward triangle from [11], filled circles from [15] and filled squares from the present reference samples.

We observe in our samples three distinct magnetic hyperfine fields around 33.2, 35.6 and 37.1 T (table 2). Almost the same low, intermediate and high fields were observed in multilayers 5/5 and 3/6 grown with the same technique as the present samples [15]. One of the main problems is then to judge on which side of the maximum field (figure 7) the low and intermediate values fall.

Assuming layer-by-layer growth without any interface roughness or interdiffusion we would for *sample 2/7* observe only one six-line pattern with a distinct Fe magnetic field corresponding to four Co atoms as nearest neighbours (nn) and two Co atoms as next nearest neighbours (nnn). Making the assumption that the sum of the Co nn and Co nnn atoms are representative for the alloy concentration of Co, this corresponds to $x \approx 0.43$ and an Fe field of about 35 T (figure 7). Now assuming roughness or intermixing, we would observe several six-line patterns each representing a special alloy situation on both sides of or close to $x \approx 0.43$.

Table 2. The magnetic hyperfine fields B_{hf} and their Gaussian distributions σ, isomer shift (δ), quadrupole shift (ϵ) and intensities (I) of the different components of all samples. Estimated errors in B_{hf} and σ are ± 0.1 T, in $I \pm 3\%$ and in δ and ϵ ± 0.01 mm s^{-1}.

Samples	2/7	3/7	5/7	9/7	14/7
$B_{hf,0}$ (T)	33.2	32.6	32.9	33.6	33.5
σ_0	1.0	0.8	1.2	0.6	0.5
I_0 (%)	46	18	33	49	65
δ_0 (mm s^{-1})	0.03	0.02	0.02	0.00	0.01
ϵ_0 (mm s^{-1})	0.02	0.02	0.02	0.00	0.00
$B_{hf,1}$ (T)	35.3	35.5	35.8	35.8	35.7
σ_1 (T)	1.0	1.4	1.1	0.8	0.9
I_1 (%)	54	62	42	51	35
δ_1 (mm s^{-1})	0.04	0.04	0.04	0.03	0.03
ϵ_1 (mm s^{-1})	−0.01	0.00	0.02	0.00	0.00
$B_{hf,2}$ (T)		37.1	37.1		
σ_2 (T)		0.7	0.9		
I_2 (%)		20	25		
δ_2 (mm s^{-1})		0.04	0.03		
ϵ_2 (mm s^{-1})		−0.04	−0.03		
Ave. sample field (T)	34.3	35.3	35.2	34.7	34.3

Table 3. Results of the fitting of the alloy samples. The notations are the same as in table 2. The Gaussian distribution parameters σ were on average about 0.80 T for each subpattern. Estimated errors in the average values are in $B_{hf} \pm 0.03$ T, in δ and $\epsilon \pm 0.003$ mm s^{-1}.

Alloy samples	$Fe_{0.75}Co_{0.25}$	$Fe_{0.50}Co_{0.50}$	$Fe_{0.25}Co_{0.75}$
B_{hf} (T)	36.59	35.06	33.27
δ (mm s^{-1})	0.037	0.037	0.026
ϵ (mm s^{-1})	0.009	0.012	0.014

The result for this sample is two six-line patterns with $B_{hf} = 33.2$ and 35.3 T. The fact that we do not observe a field of about 36.6 T, the maximum value in figure 7, is a strong indication that the observed fields correspond to x values larger than 0.27. Using figure 7 we can draw the conclusion that the observed fields correspond to $x \approx 0.73$ and $x \approx 0.46$, respectively.

Making the same analysis for the *sample 3/7* we arrive at a discrepancy between the observed high field, 37.1 T, for this multilayer and the maximum field valid for the alloys 36.6 T. Figure 7 displays the average value for the magnetic hyperfine field for a certain concentration, while the multilayer value might be representative for a special concentration of Co atoms in the neighbourhood. Narayanasamy and co-workers [7] have convincingly shown that the magnetic field distribution for an $Fe_{0.5}Co_{0.5}$ alloy sample extends between 31.7 and 37.7 T with a maximum at 34.8 T. In our alloy sample $Fe_{0.75}Co_{0.25}$ we observe a component having a field of 37.0 T. Fields larger than the average maximum field of 36.6 T have thus been observed. Furthermore, the observed small compression (on average about 2%) of the Fe near surroundings both in-plane and out-of-plane may lead to a slight change in the magnetic hyperfine field. We assume therefore that the high field component is representative for an Fe atom with a nn Co concentration of about 27%. The observed magnetic hyperfine fields 32.6, 35.5 and 37.1 T (table 3) are therefore representative for Co concentrations of about 0.81, 0.44 and 0.27, respectively.

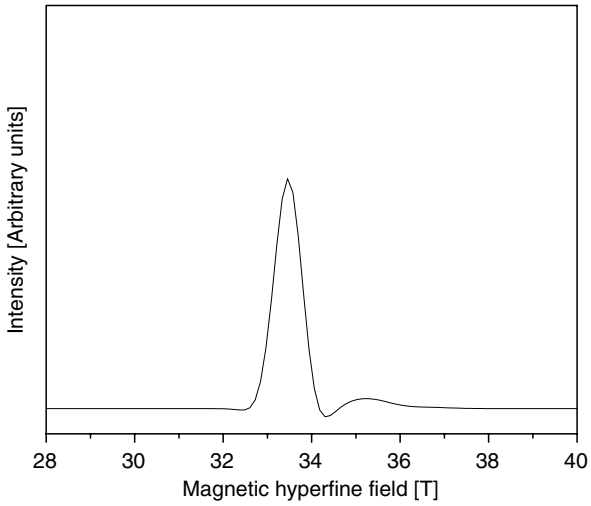

Figure 8. The scaled magnetic hyperfine field difference between the 14/7 and the 9/7 samples.

The observed magnetic hyperfine fields for *sample 5/7* are very close to the ones for sample 3/7. The major difference is the change in intensity for the different components. Here it seems that about one-third of all Fe nuclei have a low field, while one-quarter of all Fe nuclei have a high field. The rest of the Fe nuclei have an intermediate field of 35.8 T. This intermediate field may however now be a result of two different near neighbour Co surroundings according to figure 7, namely Co concentrations of 0.42 or/and 0.16.

For the *9/7 and 14/7 samples* we only observe the intermediate and low field components. For good reason we assume the ^{57}Fe Mössbauer signals from the 9/7 and 14/7 samples to have a common part, i.e. the signal from the 9/7 sample. The difference between the signals would then be emanating from the innermost five ^{57}Fe layers in sample 14/7. Making a difference plot of the hyperfine field distribution we see that this difference is a rather sharp line centred at around 33.5 T (figure 8). This field would then be representative for Fe surroundings of almost purely Fe atoms as nn and nnn. We note a slight deviation from the alloy curve since the field for Fe in α-Fe is 33.0 T.

Left to explain is then the signal from the 9/7 sample, where we observe a low field and an intermediate field component of almost the same intensity. It is not quite clear from which Co concentration the fields emanate. The low field may partly come from Co poor ($\sim$0.05) and/or Co rich ($\sim$0.67) surroundings. The intermediate field may on the other hand be an effect of a Co concentration of 0.16 and/or 0.42. It is a bit astonishing that the high field component is not seen for these samples. The reason may be that the number of Fe atoms having that alloy concentration in the near surroundings is too low to be observed as a separate pattern.

5.3. Isomer shifts

The ambiguity in Co concentration for a certain Fe magnetic hyperfine field obvious from figure 7 could be resolved when taking other hyperfine parameters into account, e.g. the isomer shift, if the Fe isomer shift shows a one-to-one relation to the Co concentration. Unfortunately, the variation of the Fe isomer shift versus Co concentration (figure 6) does not show such a relation, but the same isomer shift could be expected for different Co concentrations. Furthermore, the resolution in isomer shifts is very small as seen in figure 6. The ambiguity

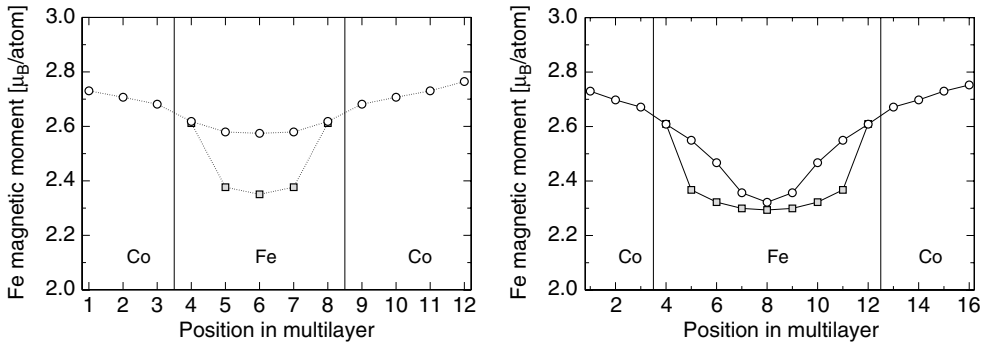

Figure 9. Calculated magnetic moments for Fe in 5/7 (left panel) and 9/7 (right panel) multilayers. Moments for both perfect (squares) and alloyed (circles) multilayers are shown. The magnetic moment is enhanced as a function of number of nearest Co neighbours. It reaches the maximum in the Co rich region in the alloyed multilayers while the moment is close to that of bulk bcc-Fe for atoms in the middle of the Fe layer of the perfect superlattices.

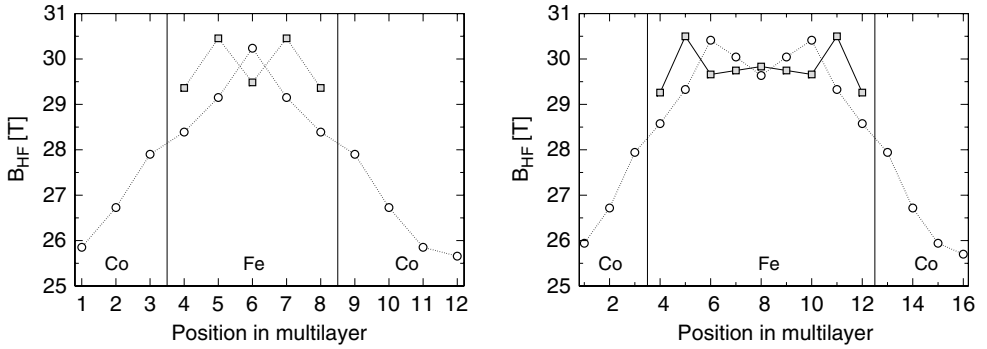

Figure 10. Calculated hyperfine fields for Fe atoms at different locations in perfect (squares) and alloyed (circles) 5/7, left panel, and 9/7, right panel, multilayers. For the perfect interface multilayers, as well as for the alloyed 9/7 multilayer, an oscillating behaviour of the hyperfine field is found. In the alloyed multilayers, the field is decreasing when the local concentration of Co increases in the Co rich region.

cannot therefore be settled. Notable however is the fact that there is a clear difference between the ordered and disordered values for the magnetic hyperfine field and isomer shift for $Fe_{0.50}Co_{0.50}$ alloys.

5.4. Experimental magnetic moments, reorientation and Fe, Co layer thicknesses

The experimental 300 K values for the magnetic moments per 'FeCo' atom (table 1) will be used to analyse the individual Fe and Co layer thicknesses for the different samples. In section 6 the measured moments will be compared with moments from a modelling of the alloying at the interface. Here we will make use of the experimental Fe, Co and alloy values for the magnetic moments [3, 36].

According to the discussion in section 5.2 the Fe atoms in *sample 2/7* have Co concentrations in the neighbourhood larger than ∼0.46. At these concentrations the Fe magnetic moment is about 3.00 μ_B. The Co moments are assumed to be invariant at about 1.79 μ_B (average value from [3]). Using these values together with the experimental value of

1.95 μ_B per 'FeCo' atom and the bilayer thickness of 9.7 ML (table 1), it is possible to estimate the experimental Fe and Co layer thicknesses to 1.4 and 8.3 ML, respectively, which is in rather good agreement with the nominal values.

As discussed in section 5.2, in the case of *samples 3/7* and 5/7 most of the Fe atoms have a Co concentration in the surroundings higher than about 0.30. An assumption of an average Fe magnetic moment of about 2.90 μ_B and a Co moment of 1.79 μ_B is therefore realistic. With the same argument as in the preceding paragraph we estimate an experimental Fe and Co layer thickness of 3.7 and 8.0 ML, respectively, for sample 3/7, and 5.1 and 7.7 ML for sample 5/7.

For *sample 9/7* the Co concentration has decreased and according to the Mössbauer data we expect an average Co concentration of about 0.10 around the Fe atoms, leading to an Fe average magnetic moment of 2.45 μ_B. Using the Co moments of 1.79 μ_B as before, the experimental Fe and Co layer thicknesses obtained are 9.8 and 8.9 ML, respectively, in rather good agreement with the nominal values.

Taking the difference between the total magnetization per bilayer for *sample 14/7* and sample 9/7 would give the net magnetization for the Fe inner layer of 14/7, assuming the Co individual layer thickness to be the same for these samples. Such an analysis gives an Fe moment of 1.30 μ_B/atom for the 5.7 Fe layers in the middle of the 15.5 Fe layers. This value is unrealistic. Assuming on the other hand that all Fe atoms have the lowest possible magnetic moment, namely 2.18 μ_B, and the Co moment of 1.79 μ_B, the experimental Fe and Co layers would be 8.8 and 15.6 ML, respectively. These values are also quite unrealistic. We have thus to conclude that the experimental magnetic moment for this sample is too low. The reason for this is unclear for the moment but errors in sample area, fewer Fe layers than nominal in the buffer layer, and the fact that the easy axis of magnetization for this sample is different to the other samples and to the applied field direction may add up to this large deviation. Assuming that the inner Fe layer would have an Fe magnetic moment of 2.18 μ_B, valid for pure α-Fe, and otherwise the sample to be similar to sample 9/7, gives 2.14 μ_B per 'FeCo atom', which is about 10% larger than the actual experimental value.

The reorientation of the in-plane easy axis from [110] to [100] shown in figure 3 has previously been observed in Fe/Co(001) superlattices [16]. Increasing the Co content increases the preference for [110] alignment, which is also observed in FeCo alloy films [37].

5.5. Calculated magnetic moments and hyperfine fields

In figure 9 the calculated magnetic moments for Fe atoms in 5/7 and 9/7 multilayers are shown. The magnetic moment for the Fe atoms is enhanced when close to Co atoms. This is in agreement with earlier experiments and calculations and the enhancement is caused by an increased spin moment due to hybridization with the Co atoms [38]. The enhancement of the spin moment is mostly limited to the interface layer. For perfect interfaces, the changes in moments for the atoms deep in the Fe layers are very small, as can be seen in the right panel of figure 9. Even for the alloyed interface, the central Fe atom has a magnetic moment close to that of bulk bcc Fe. These results show that the short-range order is what decides the size of the Fe moments. We find that the dominant factor is the number of nn Co atoms while the number of nnn only contribute very little to the spin enhancement of the Fe atoms. It can be noted that the total magnetic moment for bulk bcc Fe is $\sim$2.3 μ_B when calculated with the present method. The Co moments are found to be constant at $\sim$1.8 μ_B throughout the multilayers.

In figure 9 the calculated magnetic hyperfine fields for Fe atoms in 5/7 and 9/7 multilayers are shown. The alloyed 5/7 multilayer has a maximum of the hyperfine field in the middle of the Fe rich part of the multilayer, with a decrease of the hyperfine field as the Co concentration increases. The perfect interface multilayers have lower fields at the interface layers and in the

centre of the Fe region, whereas the intermediate layers have a higher field. This behaviour is also seen for the alloyed 9/7 multilayer. The oscillatory behaviour of the hyperfine fields shows that, contrary to the behaviour of the magnetic moments, the hyperfine field depends not only on the nearest neighbours but on the chemical order of atoms further away. From the calculated Fe hyperfine fields for the 9/7 multilayer with perfect interfaces, shown in the right panel of figure 10, it can be seen that it is in fact the composition of nn as well as nnn that contribute most to the hyperfine field, while neighbours further away play a minor role. If the hyperfine field is divided up in the valence and core contributions it is found that the core contribution is linearly dependent on the 3d spin moments, while the valence contribution varies quite linearly with the magnetic moment of the 4s electrons.

Our results also show that the calculated hyperfine fields do not reproduce the experimental values. Compared with experimental data, our method underestimates the B_{hf} for bulk bcc Fe by ∼3 T and the B_{hf} for Fe in bcc Co [12] is overestimated by ∼4 T. This can be explained by the limitations of the approximations made within the LSDA and the ASA, but also by the fact that we only calculate the Fermi contact contribution to the hyperfine field. The oscillating behaviour seen for the perfect interfaces in both 5/7 and 9/7, as well as for the 9/7 multilayer with interface alloying, can be explained by the non-linear behaviour of the B_{hf} for Fe in bulk Fe–Co alloys, as shown earlier in figure 7. This indicates that though the magnitude of the calculated hyperfine fields differs quite substantially from the experimental values, the experimental trends are reproduced.

As the differences of the hyperfine fields between the perfect and alloyed interfaces show, the hyperfine field is very sensitive to the interface quality and with the information obtained from the experimental results, it should be possible to give a good estimate of the interface alloying. Previous works on multilayers [20, 21] have successfully combined experimental data, such as magnetic moments and interlayer exchange coupling, with results obtained from electronic structure calculations for different models of interface quality, and by finding the theoretical values that agree best with the experiments the interface quality can be deduced. However, our theoretical values of the hyperfine fields seem to be systematically lower than the experimental values and a direct comparison between calculated and measured values would thus prove to be too inaccurate to allow such a procedure. For this reason, we propose a different approach, using experimental values for obtaining information on the interface quality.

6. Modelling of the magnetic effects of interface alloying

Since the theoretical values are not suitable for a direct comparison with the measured values in this study, we use experimental data for systems similar to the studied Fe/Co multilayers as reference when determining the degree of interface alloying. As we note in our calculations, the B_{hf} seem to depend strongly on the chemical composition of the nn and nnn, the local concentration. As the behaviour of the B_{hf} of Fe in disordered bulk Fe–Co alloys is well known, it should be possible to extract an expected field for a given averaged local concentration for the examined Fe atoms. If the concentration profile of the multilayer is modelled, the local concentrations can easily be found and, from known bulk data, a distribution of possible hyperfine fields can be obtained. The data used for the bulk alloys are displayed in figure 7. The experimental data have been parametrized to a sixth-degree polynomial for simple mapping of the modelled local concentration to expected fields. We have also used the same approach to model the magnetic moments as a function of interface alloying. For the magnetic moments we have parametrized the data of Kouvel [36] for the Fe moments while the Co moments have been fixed at 1.7 μ_{B} in accordance with recent results for Fe/Co multilayers [19].

In order to keep the interface modelling simple and easily understood, we have chosen to use a normal distribution of the interface alloying. This can be thought of as if every atom in

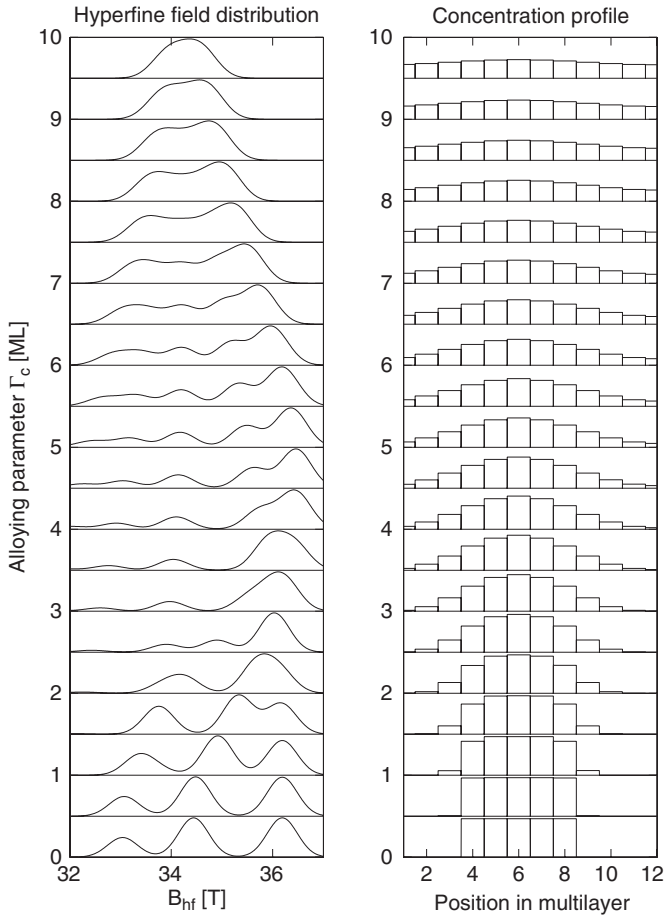

Figure 11. Hyperfine field distributions for various degrees of interface alloying for a 5/7 multilayer. Closest resemblance with experiments is obtained for an alloying parameter of ∼2 ML.

the multilayer, both Fe and Co, has the same diffusion rate in every direction of the layer. For a given diffusion rate, atoms will migrate throughout the multilayer and the averaged diffusion lengths can be described by a Gaussian distribution. These Gaussian distributions are achieved by convoluting the starting concentration profile (with perfect interfaces) with Gaussian functions with varying standard deviations. This procedure makes it possible to express the interface alloying with only one variable, the alloying parameter Γ_C expressed in ML, corresponding to the full width at half maximum of the convoluting Gaussian function. From the convoluted concentration profile, the local concentration for an Fe atom in a chosen layer is constructed by calculating the average concentration of its nearest and next nearest neighbours. The local concentration can then, from the data in figure 7, be used to determine a corresponding value of the B_{hf} for Fe atoms in the chosen layer. Summing over all layers, and weighting with the Fe concentration in each layer, results in a modelled distribution of B_{hf}. The procedure, described above, yields a set of sharp, discrete peaks of the modelled B_{hf}, with heights proportional to the expected intensity, when the field distribution is plotted. In order to more easily compare the simulated distribution with the experimental distribution (figure 5), the simulated distribution has been broadened to mimic the resolution of the measurements.

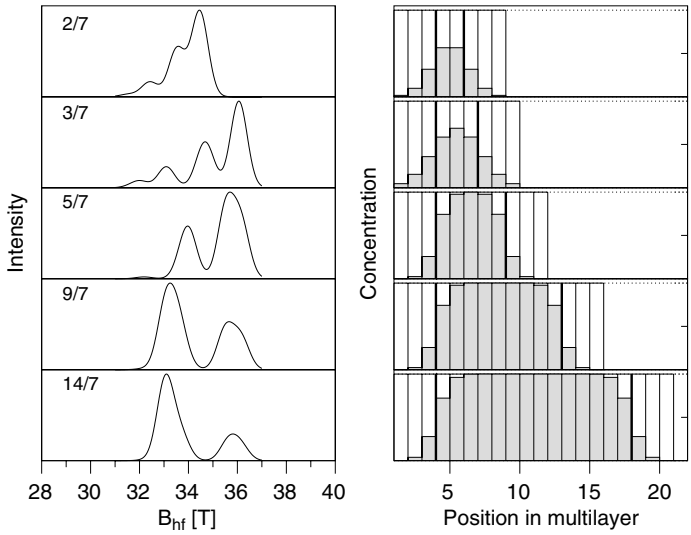

Figure 12. Fe hyperfine field distributions (left) and the Fe concentration, marked as grey bars (right), for multilayers with modelled interface alloying. The vertical dark lines indicate the original Fe layers. For the two smaller multilayers an alloying parameter of ∼3 ML is found, whereas the three thicker multilayers have a alloying parameter of ∼2 ML.

In figure 11 the field distribution and concentration profile for increasing degrees of alloying in 5/7 multilayers is shown. For $\Gamma_C = 0$ ML, which corresponds to perfect interfaces, three peaks at 33, 34.5 and 36.2 T are observed. The peak at 33 T comes from the bulk-like interior region of the Fe rich part of the multilayer, while the two other peaks come from interface layers. As the interface alloying increases, peaks are shifted and new peaks occur at 34 T for $\Gamma_C = 2$ ML and at 32.5 T for $\Gamma_C = 4$ ML. By comparison with the experimental spectra in figure 5 we find that the closest resemblance is achieved for a value of Γ_C corresponding to ∼2 ML. This choice of Γ_C for sample 5/7 corresponds to an Fe concentration distribution close to the interface in the form of 2%, 25%, 75%, 98% and 100%.

The same procedure was also performed for the other multilayer systems, and the optimal choices of Γ_C were found to be ∼3 ML for 2/7, ∼3 ML for 3/7, ∼2 ML for 9/7 and ∼2 ML for the 14/7 multilayer. The obtained concentration profiles and corresponding hyperfine field distributions can be found in figure 12.

As mentioned above, the simulated concentration profiles can also be used to predict the magnetic moment of the multilayers. In figure 13 the magnetic moments for all considered samples are shown. We see that the moments increase with increased interface alloying. For large values of the alloying parameter, the multilayers have almost complete disorder and the moments remain unchanged with the values corresponding to that of bulk alloys. Compared to hyperfine field distributions obtained by the interface alloying modelling, the modelled magnetic moments changes less dramatically. With the data obtained from the SQUID measurements, it should be possible to derive the alloying parameter from our modelled moment curves. We find for the 5/7 sample a Γ_C of ∼6 ML, and for the 9/7 sample a Γ_C of ∼2 ML, but for the other samples no suitable value was found. The discrepancies between the modelled moments and the SQUID measurements are probably due to the fact that the nominal and experimental thicknesses are not equal (see section 5.4) and that the actual Co moments are not known.

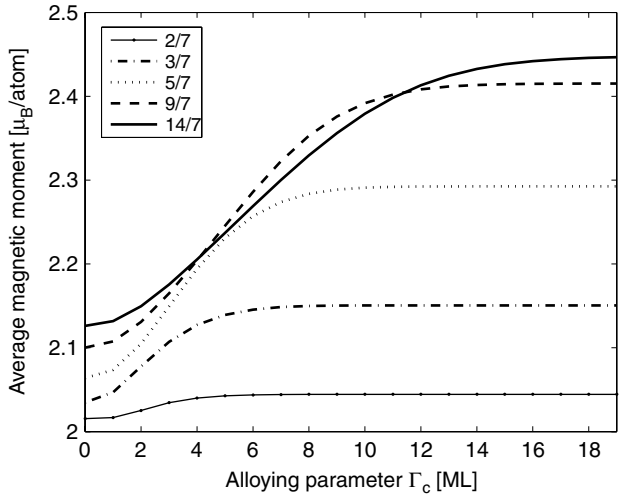

Figure 13. Magnetic moments as a function of increasing interface alloying for 2/7, 3/7, 5/7, 9/7 and 14/7 multilayers.

7. Conclusion

In this paper the magnetic hyperfine field in different regions of Fe layers in Fe/Co superlattices has been studied. It has been shown that the magnitude of the magnetic hyperfine field at the Fe atoms is increased in moving from the interface to a maximum in the second and third monolayers and then decreases to lower values on moving to the deeper part of the Fe layers, where Fe atoms are surrounded by Fe atoms only. By simulating the intermixing at the interfaces and comparing to the experimental values for the magnetic hyperfine fields from Mössbauer spectroscopy and the magnetic moments from SQUID magnetometry, the degree of intermixing is deduced to be two to three monolayers at each interface.

Acknowledgments

Matts Björck, Therese Eriksson and Sabina Ronneteg are acknowledged for their help in making the alloy samples. The Swedish Foundation for Strategic Research (SSF) is acknowledged for the support. Parts of the calculations were performed at the National Supercomputing Centre (NSC) and High Performance Computing Centre North (HPC2N). Sonia Frota-Pessôa is acknowledged for fruitful discussions regarding the electronic structure calculations.

References

[1] Kittel C 1996 *Introduction to Solid State Physics* 7th edn (New York: Wiley)
[2] Burkert T, Nordström L, Eriksson O and Heinonen O 2004 *Phys. Rev. Lett.* **93** 027203
[3] Collins M F and Forsyth J B 1963 *Phil. Mag.* **8** 401
[4] Johnson C E, Ridout M S and Cranshaw T E 1963 *Proc. Phys. Soc.* **81** 1079
[5] McGuire T R and Bardos D I 1969 *J. Appl. Phys.* **40** 1371
[6] Vincze I, Campbell I A and Meyer A J 1974 *Solid State Commun.* **15** 1495
[7] Narayanasamy A, Nagarajan T, Muthukumarasamy P and Radhakrishnan T S 1979 *J. Phys. F: Met. Phys.* **9** 2261
[8] deMayo B 1981 *Phys. Rev.* B **24** 6503

[9] Fultz B 1988 *Hyperfine Interact.* **41** 607
[10] Hamdeh H H, Fultz B and Pearson D H 1989 *Phys. Rev.* B **39** 11233
[11] Dekoster J, Jedryka E, Wójcik M and Langouche G 1993 *J. Magn. Magn. Mater.* **126** 12
[12] Dekoster J, Bemelmans H, Degroote S, DeWachter J, Jedryka E, Moons R, Vantomme A and Langouche G 1995 *Hyperfine Interact.* **95** 191
[13] Niklasson A M N and Johansson B 1999 *Phys. Rev.* B **59** 6373
[14] Lindgren B, Andreeva M, Häggström L, Semenov V G, Kalska B, Chumakov A I, Leupold O and Rüffer R 2001 *Hyperfine Interact.* **136/137** 439
[15] Häggström L, Kalska B, Nordström E, Blomqvist P and Wäppling R 2002 *J. Alloys Compounds* **347** 252
[16] Blomqvist P, Wäppling R, Broddefalk A, Nordblad P, Velthuis S G E and Felcher G P 2002 *J. Magn. Magn. Mater.* **248** 75
[17] Blomqvist P and Wäppling R 2003 *J. Cryst. Growth* **252** 120
[18] Eriksson O, Bergkvist L, Holmström E, Bergman A, LeBacq O, Frota-Pessoa S, Hjövarsson B and Nordström L 2003 *J. Phys.: Condens. Matter* **15** 599
[19] Björck M, Andersson G, Lindgren B, Wäppling R, Stanciu V and Nordblad P 2004 *J. Magn. Magn. Mater.* **284** 273
[20] Holmström E, Nordström L, Bergqvist L, Skubic B, Hjörvarsson B, Abrikosov I A, Svedlindh P and Eriksson O 2004 *Proc. Natl Acad. Sci.* **101** 4742
[21] Andersson G, Blixt A M, Stanciu V, Skubic B, Holmström E and Nordblad P 2003 *J. Magn. Magn. Mater.* **267** 234
[22] Uzdin V M and Häggström L 2005 *Phys. Rev.* B **72** 24407
[23] Isberg P, Svedberg E B, Hjörvarsson B, Wäppling R and Hultman L 1997 *Vacuum* **48** 483
[24] Ellis W C and Greiner E S 1941 *Trans. Am. Soc. Met.* **29** 415
[25] Prinz G A 1985 *Phys. Rev. Lett.* **54** 1051
[26] Nordling C and Österman J 1980 *Physics Handbook* (Lund: Studentlitteratur)
[27] Bozorth R M 1978 *Ferromagnetism* (New York: IEEE)
[28] Peduto P R, Frota-Pessôa S and Methfessel M S 1991 *Phys. Rev.* B **44** 13283–90
[29] Haydock R 1980 *Solid State Physics* vol 35 (New York: Academic) p 216
[30] von Barth U and Hedin L 1972 *J. Phys. C: Solid State Phys.* **5** 1629–42
[31] Beer N and Pettifor D G 1984 *The Electronic Structure of Complex Systems* (New York: Plenum)
[32] Petrilli H M and Frota-Pessôa S 1993 *Phys. Rev.* B **48** 7148–53
[33] Frota-Pessôa S and Legoas S B 2001 *Hyperfine Interact.* **133** 207–19
[34] Söderlind P, Eriksson O, Johansson B, Albers R C and Boring A M 1992 *Phys. Rev.* B **45** 12911–6
[35] Soroka I L, Brucas R, Stanciu V, Nordblad P and Hjörvarsson B 2004 *J. Magn. Magn. Mater.* **277** 228
[36] Kouvel J S 1969 *Magnetism and Metallurgy* vol 2 (New York: Academic) pp 523–75
[37] Mühge T, Zeidler T, Wang Q, Morawe C, Metoki N and Zabel H 1995 *J. Appl. Phys.* **77** 1055
[38] Bergman A, Holmström E, Niklasson A M N, Nordström L, Frota-Pessôa S and Eriksson O 2004 *Phys. Rev.* B **70** 174446